J. Nano- Electron. Phys.
3 (2011) No1, P. 747-754

PACS numbers: 78.20.Bh, 73.40.Lq, 84.60.Jt

SIMULATION OF CIGS THIN FILM SOLAR CELLS USING AMPS-1D

***J.R. Ray*[1], *C.J. Panchal*[1], *M.S. Desai*[1], *U.B. Trivedi*[2]**

[1] Applied Physics Department, Faculty of Technology and Engineering. M. S. University of Baroda, Vadodara-390001, India
E-mail: cjpanchal_msu@yahoo.com

[2] Department of Electronics, Sardar Patel University,
Vallabh Vidhyanagar-380120, India

The solar cell structure based on copper indium gallium diselenide (CIGS) as the absorber layer, cadmium sulfide (CdS) as a buffer layer un-doped (i) and Aluminium (Al) doped zinc oxide (ZnO) as a window layer was simulated using the one dimensional simulation program called analysis of microelectronic and photonic structures (AMPS-1D). In the simulation, the thickness of CIGS layer was varied from 300 *to* 3000 *nm. The rest of layer's thicknesses were kept constant, viz.* 60 *nm for CdS, and* 80 *nm and* 500 *nm for i- and Al-ZnO, respectively. By varying thickness of CIGS layer the simulated device performance was demonstrate in the form of current-voltage (*I-V*) characteristics and quantum efficiency (QE).*

Keywords: *CIGS THIN FILM, AMPS-1D SIMULATION, CONVERSION EFFICIENCY, QUANTUM EFFICIENCY.*

(Received 04 February 2011, in final form 14 October 2011)

1. INTRODUCTION

The copper indium gallium diselenide, $CuIn_{1-x}Ga_xSe_2$ (CIGS), based solar cells have largest efficiencies on the laboratory scale [1] and as well as on the level of large-area modules [2]. In addition to high efficiencies, CIGS thin-film modules exhibit excellent outdoor stability [3] and radiation hardness [4, 5]. Therefore, this combination of high efficiency coupled with stability and radiation hardness makes CIGS a promising material for the low cost, high efficiency solar cells. Recently, Bloss et al. [6] have predicted a conversion efficiency (η) of 33.9 % for CGS / CIS tandem solar cells at global air mass (AM) 1.5 illuminations. Song et al. have modeled a CGS / CIGS tandem solar cell and they have shown that η was 25 % achievable when a high efficiency CGS top cell was used with an optimized CIGS bottom cell [7].

In this present work, a one dimensional simulation program called a analysis of microelectronic and photonic structures (AMPS-1D) [8] is used to simulate the $CuIn_{1-x}Ga_xSe_2$: $x = 0.3$ solar cell structure. Fig. 1 shows the schematic of solar cell design studied in this work. The aim of the simulation of CIGS solar cell structure was to check the device performance by varying the thickness of the CIGS absorber layer. The device performance is mainly based on the material parameters, optical parameters, and electrical parameters of each layers used in the structure. In this simulation the required parameters of CIGS thin film having a thickness of 300 nm were taken from the elsewhere [9]. For the rest of the layers the standard parameters [10] were used.

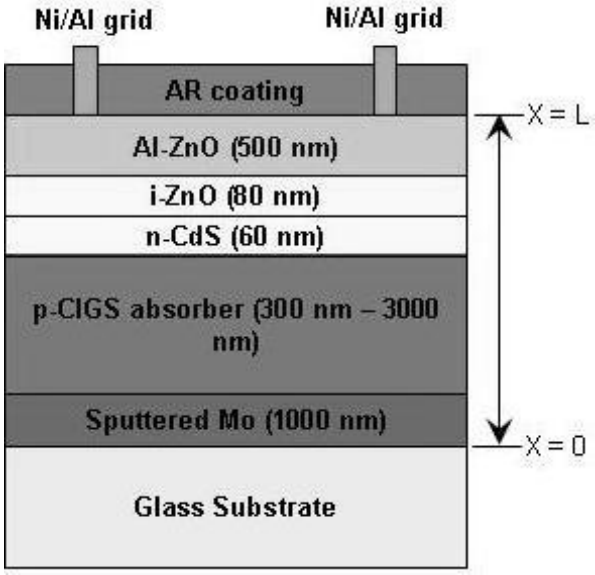

Fig. 1 *– CIGS solar cell structure used for the simulation*

The thickness of the CIGS, in general, was kept ~ 2000-2500 nm [11, 12] in the commercial available solar cell device. In concern with that in this work, we simulate the solar cell structure by increasing the thickness of CIGS from 300 to 3000 nm. It was found from the simulated results that the η, and quantum efficiency (QE) were considerable influenced by the absorber layer thickness. As the thickness of the absorber layer increases from 300 to 3000 nm, the value of η increases from 8.25 % to 10 % and the response of QE improves near to the band edge of CIGS.

2. MODEL DISCRIPTION

The AMPS software can operate in two distinct modes: the density of state (DOS) mode or the lifetime mode. A description of both modes can be found in the AMPS manual [8]; a comparative discussion is found in A. L. Fahrenbruch's work on CdTe solar cells [13]. In essence, the lifetime mode accepts inputs in the form of carrier lifetimes, which are assumed constant, independent of light and voltage bias, and does not address the underling recombination processes. The DOS mode allows the definition of multiple defect states, using densities, energy distributions, and capture cross-sections. Based on this information, the recombination current and defect occupancy is calculated using the Shockley-Read-Hall formalism.

To model the charge transport processes in the present structure shown in Fig. 1, the drift-diffusion approach is used as a function of device length, x. The three main equations are: the Poisson's equation, continuity equation for free holes, and continuity equation for free electrons. Generally, the Poisson's equation is [14]:

$$\frac{d}{dx}\left(-\varepsilon(x)\frac{d\psi}{dx}\right) = q\left[p(x) - n(x) + N_D^+(x) - N_A^-(x) + p_t(x) - n_t(x)\right] \qquad (1)$$

where, ψ is the electrostatic potential, n, p are the concentrations of free electrons and holes, n_t, p_t are the concentrations of trapped electrons and holes, N_D^+, N_A^- are the concentrations of ionized donors and acceptors, ε is the dielectric permittivity of semiconductor, and q is the electron charge.

The transport characteristics of an electronic device may be derived by the continuity equation for the holes and electrons. The continuity equations in steady state conditions are:

$$\frac{1}{q}\frac{dJ_n}{dx} = R_n(x) - G(x), \tag{2}$$

$$\frac{1}{q}\frac{dJ_p}{dx} = G(x) - R_p(x) \tag{3}$$

where, J_n, J_p are electron and hole current density, R_n, R_p are electrons and holes recombination velocities for direct band-to-band and indirect transitions, and G is the optical generation rate which is expressed as a function of x is,

$$G(x) = -\frac{d}{dx}\sum_i \Phi_i^{FOR}(\lambda_i) + \frac{d}{dx}\sum_i \Phi_i^{REV}(\lambda_i) \tag{4}$$

where, Φ_i^{FOR} and Φ_i^{REV} are, respectively, the photon flux of the incident light and the light reflected from the back surface at a wavelength, λ of i at some point x, depending on the light absorption coefficient, and the light reflectance in the forward and reverse direction. In our simulation, the reflection indices for the forward and reverse directions are 0 and 0.6, respectively. The governing equations (1), (2), and (3) must hold at every position in a device, and the solution to these equations involves determining the state variables $\psi(x)$, the n-type quasi-Fermi level E_{Fn}, and the p-type quasi-Fermi level E_{Fp} or, equivalently, $\psi(x)$, $n(x)$, and $p(x)$, which completely defines the system at every point x. Because the governing equations for $\psi(x)$, E_{Fn}, and E_{Fp} are non-linear and coupled, they cannot be solved analytically. There must be boundary conditions imposed on the set of equations. The Newton-Raphson technique is used in AMPS-1D. To be specific, the solutions to equations (1), (2), and (3) must satisfy the following boundary conditions:

$$\begin{aligned}
&\Psi(0) = \Psi_0 - V;\\
&\Psi(L) = 0;\\
&J_p(0) = -qS_{po}[p_o(0) - p(0)];\\
&J_p(L) = qS_{pL}[p(L) - p_o(L)];\\
&J_n(0) = qS_{no}[n(0) - n_o(0)];\\
&J_n(L) = -qS_{nL}[n_o(L) - n(L)].
\end{aligned} \tag{5}$$

S_{po}, S_{pL}, S_{no}, and S_{nL} appearing in those conditions are effective interface recombination speeds for holes and electrons at $x = 0$, and $x = L$.

AMPS-1D solves three coupled differential equations each subject to boundary conditions (equation. 5) and then calculates the electrostatic potential and the quasi-Fermi level for holes and electrons at all point in the solar cell. Once these values are known as a function of depth, it is straightforward to calculate the carrier concentrations, electric fields and currents, and device parameters like the open-circuit voltage (V_{oc}), short-circuit current density (J_{sc}), fill-factor (FF), and the efficiency (η). These parameters define the performance of a solar cell.

The grid spacing was selected to be denser in the thinner top layers of the device, where more rapid changes are to be expected in the band structure. The grid point does not exceed the maximum limit of 400. Selected biases were entered as necessary; by default AMPS calculates QE and band structure for thermodynamic equilibrium, maximum power point, and under open-circuit conditions.

3. EXPERIMRNTAL

In this study, a one-dimensional numerical analysis tool, AMPS-1D, is used to create various solar cell models and obtain its results. In AMPS-1D, four different layers are required for the modeling. More layers can be added as long as the grid points do not exceed the limitation, viz. 400-grid points. The four layers that are used in this modeling is the n-type Al doped ZnO, i-ZnO, CdS and CIGS. Table 1 and Table 2 show the description for the parameters used in the simulation and the base parameter that are used throughout the study [10].

Table 1 *– Parameters used for the CIGS solar cell simulation*

Layers / Parameters	n^+-ZnO	$n(i)$-ZnO	CdS	CIGS
Thickness (μm)	500	80	60	300*- 3000
Dielectric constant, ε	9	9	10	13.6
Electron mobility, μn (cm^2/Vs)	50	50	6	300
Hole mobility, μ_p(cm^2/Vs)	5	5	3	36*
Carrier density, n or p (cm^{-3})	n:1.70E+19	n:5E+16	n:6E+16	p:2.0E+17*
Optical band gap, E_g (eV)	3.3	3.3	2.4	1.20*
Effective density, N_c (cm^{-3})	1.00E+19	1.00E+19	1.00E+19	3.00E+18
Effective density, N_v (cm^{-3})	1.00E+19	1.00E+19	1.60E+19	1.50E+19
Electron affinity, χ (eV)	3.9	3.9	3.75	4.15

* parameters of CIGS thin films grown by flash evaporation method on soda lime glass substrate [9].

The front and back contacts are solely defined by their work function and the reflectivity of the contact-semiconductor interface: work function for front contact is 0 eV i.e. at the Fermi level E_F and the reflectivity is 0.3.

Similarly 0.9 eV work function i.e. above E_F and reflectivity is 0.8. The AM 1.5 G photon flux was used for the illumination (Fig. 2). The number of incident photons / (cm^2/s) was entered for wavelengths between 250 nm to 2500 nm, with a step size of 2 nm. The front panel of AMPS-1D simulation for CIGS solar cell structure is shown in Fig. 3.

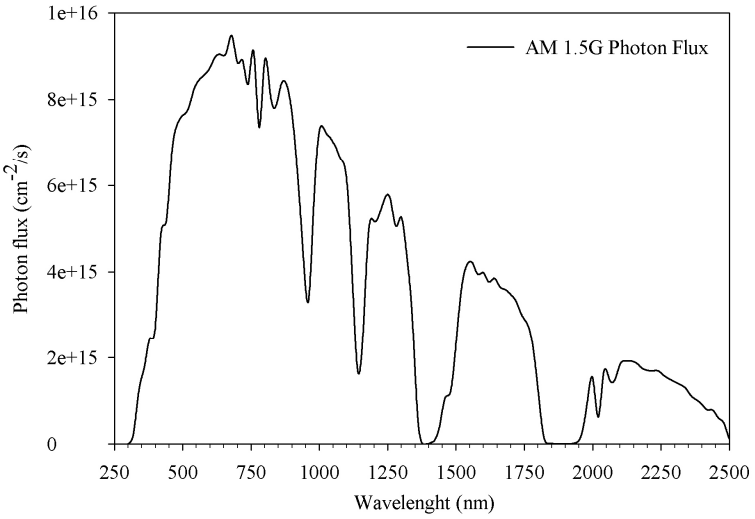

***Fig. 2** – AM1.5G photon flux as the illumination*

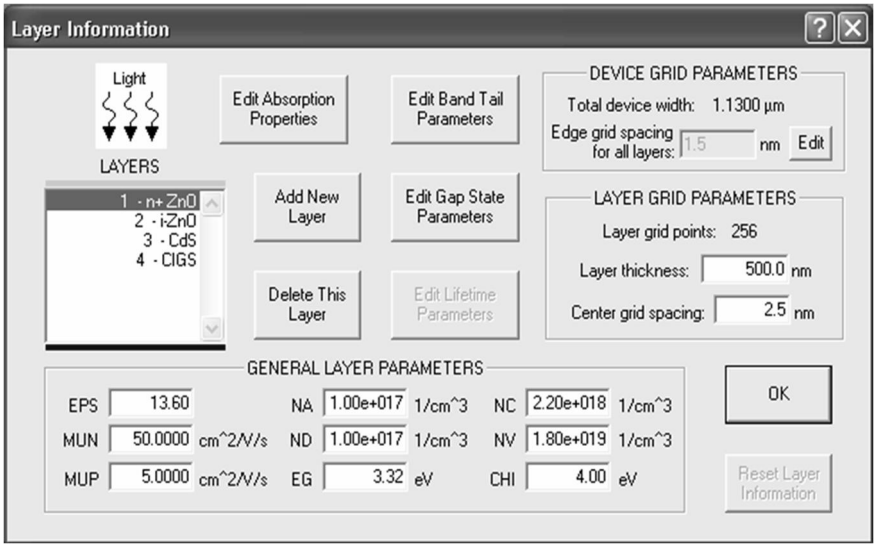

***Fig. 3** – AMPS simulation front panel contains the device and layer grid parameters, and general layer parameters*

4. RESULTS AND DISCUSSIONS

CIGS solar cells have a complex multilayer structure. Cell analysis is also complexed by a complicated window structure, consisting of a thin buffer layer (CdS or an alternative) and a double TCO layer (e.g. nominally undoped ZnO followed by Al doped ZnO). It is clear that numerical modelling is necessary to evaluate quantitatively the effect of a set of assumed input parameters. Fig. 4 (*a*) shows the J-V characteristic, using AMPS-1D, of the CIGS solar cell structure having a different thickness of CIGS absorber layer. As the thickness of the layer increases from 300 nm to 3000 nm, the conversion efficiency increases from 8.25 % to 10 %. Fig. 4 (b) shows the variation in the V_{oc} and I_{sc} including η as a function of absorber thickness. It indicates that below 1500 nm thickness of absorber the cell shows the sharp decrease in the V_{oc}, I_{sc} and therefore decrease in the η. The cell having a 300 nm thick CIGS indicates 0.452 volt is V_{oc} and I_{sc} is 25.4 mA/cm^2.

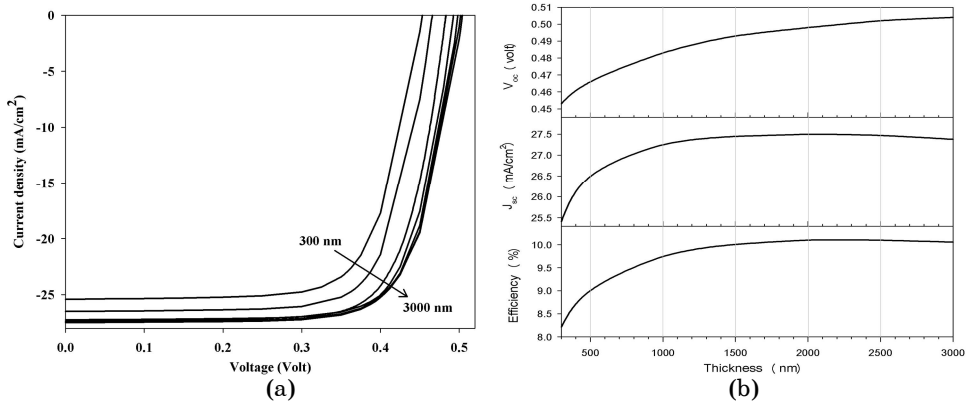

(a) (b)

***Fig. 4** – (a) J-V spectra for different CIGS thicknesses shows that the efficiency increases as the thickness increases and saturates after* 1500 *nm (b) Variation in the V_{oc}, J_{sc}, and efficiency as a function of CIGS thickness shows that the CIGS thinner the CIGS layer below* 2000 *nm the considerable decreases in the V_{oc}, J_{sc}, and so, in the efficiency of the solar cell*

The spectral response shown in Fig. 5 indicates the absorber having a lower, 300 nm, thickness loose a part of J_{sc} near to the band edge (~ 1000 nm) of the CIGS.

As the thickness of the absorber layer increases, the recombination probability of the photon-generated carriers with back-contact is decreases. Recombination is mainly depend on the junction depth. As the thickness of the layer increases, the junction depth decrease relative to the thickness of the layer. Therefore, the photogenerated carriers are collected efficiently at higher thickness of the absorber layer. QE spectra shown in Fig. 5 suggest that at higher thickness of the CIGS absorber layer the maximum photon generated carriers are being collected and gives maximum ~ 70 % photon conversion efficiency.

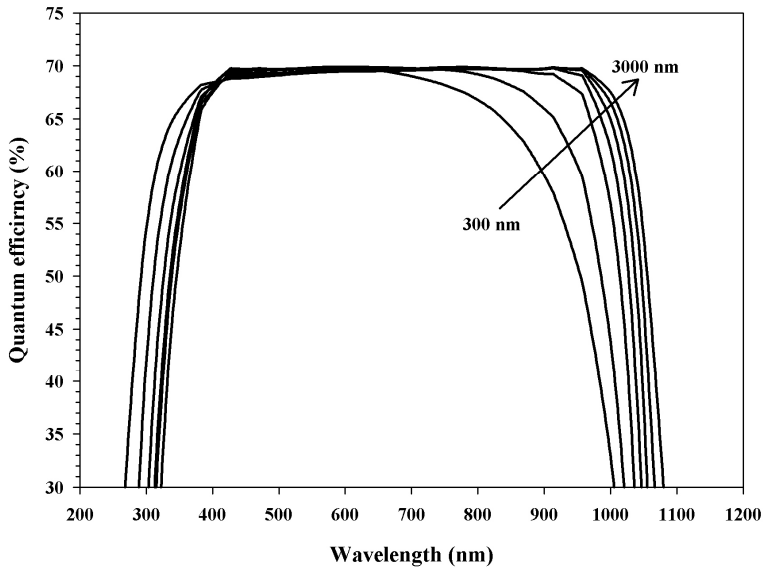

Fig. – 5 *QE spectra for different CIGS thickness shows that higher thickness absorbs more photons which improves the overall efficiency of the device*

5. CONCLUSIONS

We have used AMPS-1D to study the dependence of absorber layer thickness for CIGS thin films solar cells. We demonstrated the effect of absorber thickness on the solar cell parameters like open-circuit voltage (V_{oc}), short-circuit current density (J_{sc}), conversion efficiency (η), and the quantum efficiency (QE). The conversion efficiency increased until the thickness reached at around 2000 nm. Further increase in the thickness of the films does not show any improvement in the efficiency. The optimum conversion efficiency is 10 % observed. Similarly response of QE is nearly overlap after the 2000 nm thickness of the CIGS absorber layer. These observation leads to the conclusion that for the optimum performance of the solar cell device the thickness of the absorber layer plays an important role.

We would like to acknowledge the use of AMPS-1D program that was developed by Dr. Fonash's group at Pennsylvania State University (PSU).

REFERENCES

1. I. Repins, M.A. Contreras, B. Egaas, C. DeHart, J. Scharf, C.L. Perkins, B. To, R. Noufi, *Prog. Photovolt: Res. Appl.* **16**, 235 (2008).
2. C. Lombardi, (http://www.miasole.com/sites/default/files/Cnet_Dec_02_2010.pdf)
3. H.S. Ullal, K. Zweibel, B.V. Roedern, *Proceedings of the 26th IEEE Spec. Conference, IEEE*, art. No. 2012 (1997).
4. M. Yamaguchi, *J. Appl. Phys.* **78,** 1476 (1995).
5. H.W. Schock, K. Bogus, in: J. Schmid, H.A. Ossenbrink, P. Helm, H. Ehmann, E.D. Dunlop (Eds.), *Proceedings of the 2nd World Conference on Photovoltaic Energy Conversion, E.C. Joint Research Centre, Luxemburg,* art. No. 3586 (1998).

6. W.H. Bloss, J. Kimmererele, F. Pfisterer, H.W. Schock, *Conference Record of the 17th IEEE PVSC*, art. No. 715 (1984).
7. J. Song, S.S. Li, C.H. Huang, T.J. Anderson, O.D. Crisalle, *NCPV and Solar Program Review Meeting*, art. No. P874 (2003).
8. S.J. Fonash, *A manual for One-Dimensional Device Simulation Program for the Analysis of Microelectronic and Photonic Structures (AMPS-1D)*, (The Center for Nanotechnology Education and Utilization, The Pennsylvania State University, University Park, PA 16802).
9. J. Ray, C.J. Panchal, *Symposium on Condensed Matter Physics (CMDAYS 09)*, art. No. P-090 413 (2009).
10. M. Gloeckler, A.L. Fahrenbruch, J.R. Sitesm, *Proceedings of 3rd World Conference on Photovoltaic Energy Conversion,* 491 (2003).
11. O. Lundberg, M. Edoff, L. Stolt, *Thin Solid Films* **480,** 520 (2005).
12. S. Ishizuka, A. Yamada, K. Matsubara, P. Fons, K. Sakurai, S. Niki, *Curr. Appl. Phys.* **10,** S154 (2010).
13. A.L. Fahrenbruch, R.H. Bube, *Fundamentals of solar cells* (NewYork: Academic Press: 1983).
14. S.M. Sze *Physics of semiconductor devices* (New York: John Wiley & Sons Press: 1981).